doi:10.1016/j.jmb.2005.06.016 J. Mol. Biol. (2005) 351, 731–748

JMB

Available online at www.sciencedirect.com

SCIENCE DIRECT®

ELSEVIER

Structural Dynamics of Precursor and Product of the RNA Enzyme from the Hepatitis Delta Virus as Revealed by Molecular Dynamics Simulations

**Maryna V. Krasovska[1,2]†, Jana Sefcikova[3]†
Nad'a Špačková[4], Jiří Šponer[4,5]* and Nils G. Walter[3]***

[1]*National Center for Biomolecular Research, Faculty of Science, Masaryk University Kotlarska 2, 611 37 Brno, Czech Republic*

[2]*Institute for Single Crystals National Academy of Sciences of Ukraine, 61001 Kharkov Ukraine*

[3]*Department of Chemistry University of Michigan 930 N. University Avenue Ann Arbor, MI 48109-1055 USA*

[4]*Institute of Biophysics Academy of Sciences of the Czech Republic, Královopolská 135, 612 65 Brno, Czech Republic*

[5]*Institute of Organic Chemistry and Biochemistry, Academy of Sciences of the Czech Republic Flemingovo n. 2, 16610 Prague Czech Republic*

**Corresponding authors*

The hepatitis delta virus (HDV) ribozyme is a self-cleaving RNA enzyme involved in the replication of a human pathogen, the hepatitis delta virus. Recent crystal structures of the precursor and product of self-cleavage, together with detailed kinetic analyses, have led to hypotheses on the catalytic strategies employed by the HDV ribozyme. We report molecular dynamics (MD) simulations (~120 ns total simulation time) to test the plausibility that specific conformational rearrangements are involved in catalysis. Site-specific self-cleavage requires cytidine in position 75 (C75). A precursor simulation with unprotonated C75 reveals a rather weak dynamic binding of C75 in the catalytic pocket with spontaneous, transient formation of a H-bond between U−1(O2′) and C75(N3). This H-bond would be required for C75 to act as the general base. Upon protonation in the precursor, $C75H^+$ has a tendency to move towards its product location and establish a firm H-bonding network within the catalytic pocket. However, a $C75H^+$(N3)-G1(O5′) H-bond, which would be expected if C75 acted as a general acid catalyst, is not observed on the present simulation timescale. The adjacent loop L3 is relatively dynamic and may serve as a flexible structural element, possibly gated by the closing U20·G25 base-pair, to facilitate a conformational switch induced by a protonated $C75H^+$. L3 also controls the electrostatic environment of the catalytic core, which in turn may modulate C75 base strength and metal ion binding. We find that a distant RNA tertiary interaction involving a protonated cytidine (C41) becomes unstable when left unprotonated, leading to disruptive conformational rearrangements adjacent to the catalytic core. A Na ion temporarily compensates for the loss of the protonated hydrogen bond, which is strikingly consistent with the experimentally observed synergy between low pH and high Na^+ concentrations in mediating residual self-cleavage of the HDV ribozyme in the absence of divalents.

Keywords: cytidine protonation; HDV ribozyme; hydration site; metal ion binding; RNA folding

Introduction

The hepatitis delta virus (HDV) is a highly infectious human pathogen that can cause acute liver inflammation and progressive chronic liver diseases.[1] The viral circular RNA genome and its complement, the anti-genome, both contain closely related structural motifs with enzyme-like activity, the two forms of the HDV ribozyme. The HDV ribozyme is essential for cleaving multimeric intermediates generated during double rolling-circle replication of the viral RNA. It utilizes several catalytic strategies for rate enhancement of the transesterification reaction that cleaves a specific phosphodiester bond.[2] One of the major catalytic strategies, general acid-base catalysis, requires

† M.V.K. and J.S. contributed equally to this work.

Abbreviations used: HDV, hepatitis delta virus; MD, molecular dynamics; RMSD, root-mean-square deviation; WC/WC, Watson–Crick/Watson–Crick; NESP, negative electrostatic potential; PDB, Protein Data Bank.

E-mail addresses of the corresponding authors: sponer@ncbr.chemi.muni.cz; nwalter@umich.edu

deprotonation of the 2′-OH nucleophile of nucleotide −1, immediately preceding the scissile phosphate, and protonation of the 5′-oxyanion leaving group of nucleotide 1, immediately downstream of the scissile phosphate (Figure 1(a)).

Two kinetically equivalent mechanisms have been proposed wherein nucleobase C75 in the genomic HDV ribozyme (or the equivalent C76 in the anti-genomic form) acts as either general base or general acid.[3,4] C75 is crucial for ribozyme activity as determined first by mutagenesis studies in which a mutation to U, G or A at this position resulted in a reduction by >100-fold in catalytic rate, more than mutations at any other position.[5–7] Crystallographic studies subsequently showed that C75 indeed is situated in proximity to the cleavage site in both the reaction precursor and 3′ product forms of the genomic HDV ribozyme.[8–10] Controversially, the conformation of the catalytic pocket in the precursor crystal led to the hypothesis of a general-base involvement of C75 in the reaction mechanism,[10] while the hydrogen (H-)bond between C75(N3) and the 5′-OH leaving group in the product crystal[8,9] is suggestive of general acid catalysis. A role of the

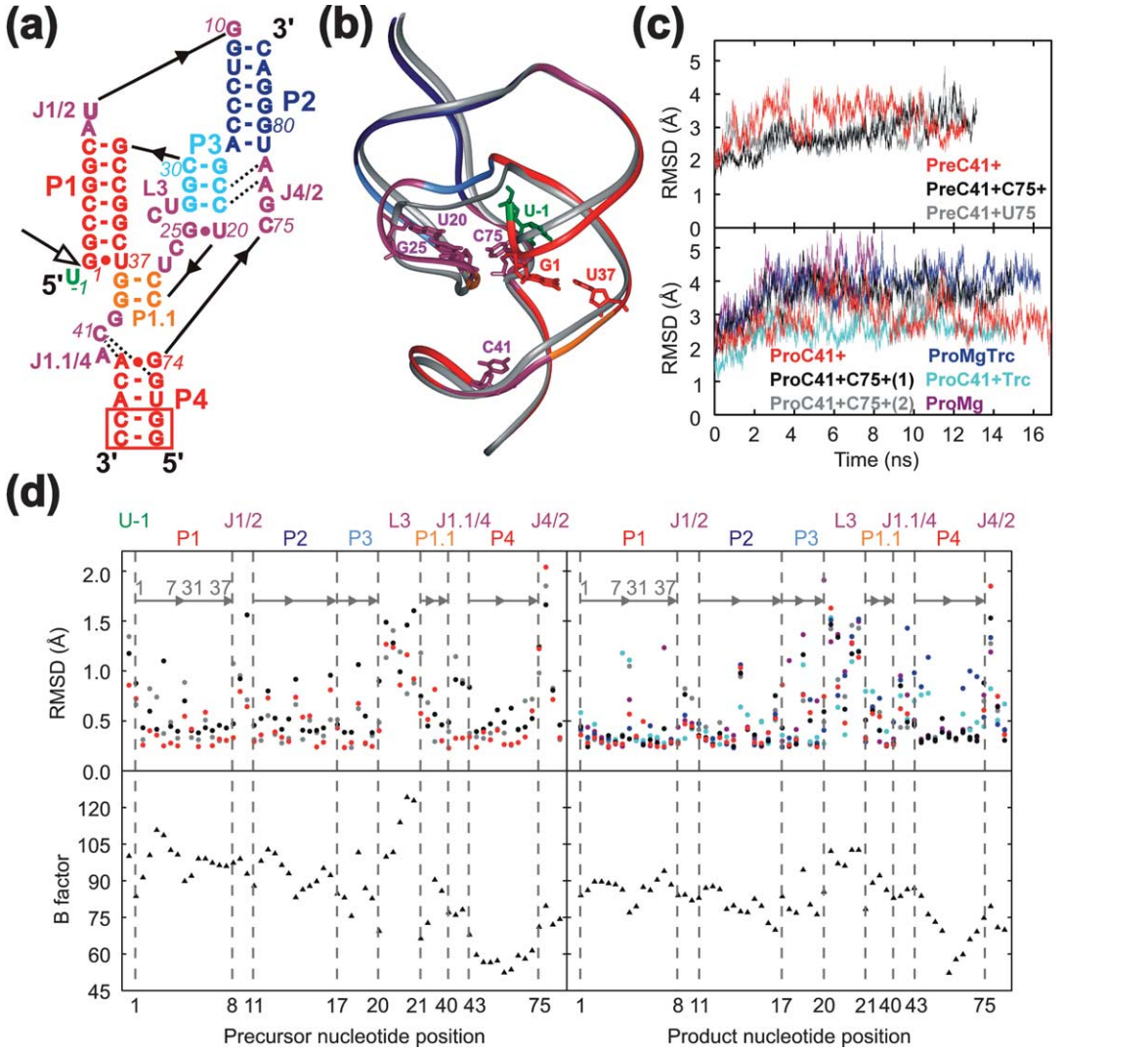

Figure 1. Overview over crystal structures and MD simulations of the precursor and product forms of the HDV ribozyme. (a) Sequence and secondary structure of the simulated genomic HDV ribozyme with structural elements color-coded. The product form lacks U−1. Open arrow, cleavage site; rectangular, two base-pairs omitted in simulations ProMgTrc and ProTrcC41+; broken lines, J1.1./4 quadruple and A-minor motifs of A77 and A78. (b) Overlap of the crystal structures of the precursor[10] (color-coded as in (a)) and product[9] (silver) with key nucleotides indicated. (c) Root-mean-square deviation (RMSD) over time of our precursor (top) and product (bottom) simulations from their respective crystal structure (RMSD of simulation ProTrcC41+ were calculated with respect to its initial structure). (d) Top panel: averaged RMSD value for each nucleotide (calculated without hydrogen atoms) of our precursor (left) and product (right) simulations (color-coded as in (c)) from their respective crystal structure (top). Bottom panel: *B* factor for each nucleotide (calculated as the average of the atomic *B* factors) in the precursor (left) and product (right) crystal structures, as obtained from the RCSB Protein Data Bank for accession codes 1SJ3 and 1CX0, respectively. The *x*-axis is organized following the secondary structure of the ribozyme, and gray arrows indicate the 5′→3′ direction of the 5′ and 3′ segments of each helix.

anti-genomic C76 as general base was supported by rescue of cleavage in a C76U mutant by imidazole with an apparent pH dependence consistent with base catalysis.[3] By contrast, the slow cleavage with inverted pH profile observed for the genomic ribozyme in the presence of divalent metal ion chelator and high Na^+ concentrations suggested a model in which C75 acts as the general acid, which becomes unmasked only in the absence of the general base, a hydrated Mg ion.[4] However, follow-up studies showed that activity at low pH and high Na^+ concentrations depends on the presence of a base quadruple involving a protonated C41, so it is not necessarily related to C75.[11] Adding to the controversy, proton inventory and kinetic solvent isotope effect experiments on the anti-genomic HDV ribozyme found that a single proton is transferred during the rate-limiting step,[12] while similar studies on the genomic ribozyme reported a two-proton transfer.[13] Finally, because catalysis is fastest around neutral pH, the pK_a value of the N3 of C75 must be substantially perturbed from that of the free base (~4.2).[14] However, using solution ^{13}C-NMR, no clear evidence for a large pK_a shift of C75(N3) was found in either the precursor or product forms of a genomic ribozyme, suggesting that C75 protonation may only occur close to the transition state.[15]

The crystal structures provide a clear, albeit static, atomistic view of the genomic HDV ribozyme (Figure 1(b)).[8–10] The global conformations of the precursor and product forms are similar; both share a compact structure comprising five helical segments, P1–P4 and P1.1, connected to form a nested double pseudoknot. The helical segments form two parallel stacks, P1|P1.1|P4 and P2|P3 (| symbolizes stacking). These stacks are tied together by three strand-crossovers (joiners J1/2, J1.1/4, and J4/2) and a loop (L3) (Figure 1(a)). This unique fold brings all necessary functional groups together to form a tight, well-defined catalytic pocket between J4/2 (carrying C75), L3, and P1.1. In the product structure, the 5′-OH leaving group is tugged into this pocket by hydrogen bonding with C75(N3).[8,9] By contrast, the precursor structures, which were derived either with an inactivating C75U mutation in the presence of divalent cations or with a wild-type C75 in the absence of divalents, depict base 75 retracted from the 5′-oxygen leaving group by ~2 Å. This conformational difference appears to be, at least in part, due to the presence of the 5′ product that wedges into the catalytic pocket to widen it, thus pushing the flanking P1|P1.1|P4 and P2|P3 stacks apart and leading to conformational rearrangements in L3 (Figure 1(b)).[10] Such a substantial conformational change from precursor to product is consistent with prior findings from fluorescence spectroscopy, NMR, and footprinting.[15–22] Only one nucleotide in the 5′ product is required for the cleavage reaction to occur,[23] and one nucleotide is all that is resolved in the precursor crystal structure, suggesting that the upstream sequence is flexible. The resolved U−1 nucleotide is bent away from G1 by a sharp ~180° turn about the scissile phosphate, resulting in a distance between U−1(O2′) and C75(N3) that is beyond H-bonding (Figure 1(b)). To interpret their crystal structure in light of the existing mechanistic models, Doudna and co-workers proposed that catalysis occurs when U−1 undergoes a rigid-body rotation, bringing its 2′-OH into H-bonding distance from C75(N3). C75 then acts as a general base catalyst to activate and position the 2′-OH for in-line nucleophilic attack on the scissile phosphate. Finally, backbone scission and departure of the 5′ product lead to a conformational switch towards the product structure that drives the reaction forward.[10]

The missing link between static crystal structures and mechanistic models of catalysis are the structural dynamics of an enzyme. Here, we complement the existing structural and biochemical data on the HDV ribozyme with ~120 ns of explicit solvent molecular dynamics (MD) simulations on both its precursor and product forms. Such explicit solvent MD simulations have been used successfully to analyze the structure and dynamics of RNA,[24–40] with only a limited number of studies directed towards ribozymes.[41–43] The structural insights from MD simulations may later be complemented by quantum chemical calculations on the catalytic mechanism.[44,45] The main goal of the present study was to evaluate the plausibility that conformational dynamics around the catalytic C75 indeed are involved in catalysis. We find that an unprotonated C75 does not establish similarly stable H-bonds in the catalytic pocket of the precursor as it does in the product. The unprotonated precursor C75(N3) does, however, form a spontaneous, if temporary H-bond with U−1(O2′) upon rotation of the very dynamic U−1 nucleotide. By contrast, upon protonation we find C75H$^+$ in the precursor to move towards its product location, establishing more stable, product-like H-bonds. Yet no G1(O5′)-C75H$^+$H-bond, as postulated in the general acid mechanism, was observed on our simulation timescale. Taken in sequence, these observations are most consistent with the conformational changes invoked for the general base catalysis mechanism. The adjacent loop L3 appears to be a particularly flexible structural element that may facilitate, perhaps gated by the closing U20·G25 base-pair, a conformational switch induced by C75H$^+$. L3 also controls the electrostatic environment of the catalytic core, which in turn likely modulates cation binding and C75 base strength. Finally, we find that a protonated C41H$^+$ is essential for stability of the base quadruple in the J1.1/4 junction, which stacks under P1.1 and the catalytic core. Association with a Na ion appears to transiently compensate for the loss of C41 protonation. This could explain the synergy between low pH and high Na^+ concentrations in mediating slow cleavage of HDV ribozymes containing J1.1/4. In general, the observed structural dynamics of the HDV ribozyme are complemented by numerous

cation binding and hydration sites, many of which involve long-residency metal ions and water molecules, respectively.[33,34]

Results and Discussion

Overview over the simulations

To assess the structural dynamics of the HDV ribozyme precursor (containing the U−1 nucleotide) in dependence of the protonation state of C75, the following three precursor simulations were performed in Na^+ as the neutralizing cation over a total length of ~40 ns (Table 1; Figure 1): simulation PreC41+(13 ns) was based on the high-resolution crystal structure of a C75U mutant precursor,[10] however, with C75 replacing the crystal structure U75. Simulations PreC41+C75+ and PreC41+U75 (each 13 ns) were carried out with an N3-protonated $C75H^+$ and with the original U75, respectively.

To test how protonation of C75 and C41 impact structural dynamics of the HDV ribozyme in the context of the 3′ product crystal structure (lacking the U−1 nucleotide), the following six simulations were performed over a total length of ~80 ns (Table 1; Figure 1): simulation ProC41+ was carried out for 15 ns in the presence of Na^+, with C41 protonated at the N3 position ($C41H^+$) and C75 left unprotonated, which directly corresponds to the unmodified 3′ product crystal structure.[9] ProC41+C75+(1) (15 ns) and ProC41+C75+(2) (13 ns) were two simulations similar to ProC41+ except that C75 was additionally protonated at the N3 position. In simulation ProMgTrc (16.5 ns) neither C41 nor C75 was protonated, nine crystallographically resolved Mg cations were included, and stem P4 was further truncated by two terminal base-pairs. Simulation ProTrcC41+(15 ns) started from a 7.5 ns snapshot of simulation ProMgTrc, in which C41 was then protonated at the N3 position and all Mg ions were removed (while neutralizing the system with Na^+) to test whether the structural impact of a C41 deprotonation observed in simulation ProMgTrc (see below) is reversible. Finally, simulation ProMg (8.2 ns) was similar to ProMgTrc, except that the P4 stem was not truncated further. Please note that we deliberately did not include Mg ions in our simulations other than for the two exceptions given above. The description of divalent cations in MD is controversial, as it neglects major polarization and charge transfer terms and samples insufficiently.[33,34]

All nine simulations exhibit stable time trajectories in which the five double-helical regions P1, P1.1, P2, P3 and P4 remain relatively close to their starting crystal structures, resulting in low overall RMSD values (Figure 1(c)). This global stability of the molecule is in agreement with its compact fold and the extensive network of H-bonding and stacking interactions (Figure 1(a); Table 2),[8,10] a large majority of which, yet not all, are preserved in our MD simulations. Figure 1(d) summarizes the RMSD value of each nucleotide relative to its position in the crystal structure. These individual RMSD values follow trends of the experimental *B* factors (Figure 1(d)), suggesting that our simulations reasonably reflect the experimental flexibility (or uncertainty) of the various segments of the HDV ribozyme in the crystal. In most cases, L3 fluctuations contribute rather significantly to the overall RMSD value (Figure 1(d)), particularly in those simulations where L3 undergoes complete or partial unfolding (PreC41+U75, ProC41+C75+(1), and ProMg; see below). Furthermore, the contribution of J1.1/4 and P4 to the overall RMSD value is significant specifically for simulations ProMgTrc and ProMg (Figure 1(d)), where C41 is unprotonated. Even with these locally enhanced dynamics, the general stability of our simulations suggests that they are rather conservative and realistic estimates of the structural dynamics of the HDV ribozyme.

Consistent monovalent cation binding sites and hydration patterns are observed among different simulations, suggesting reasonable sampling.[33,34,46,47] Cation and water binding sites associated with

Table 1. Overview over simulations carried out in this study

Simulation	Starting structure	Number of nucleotides	Protonation state	Duration (ns)	Presence of ions
PreC41+	Precursor[a]	63	$C41H^+$/C75	13	60 Na^+
PreC41+C75+	Precursor[a]	63	$C41H^+$/$C75H^+$	13	59 Na^+
PreC41+U75	**Precursor[a]**	**63**	**$C41H^+$/U75**	**13**	**60 Na^+**
ProC41+	**Product[b]**	**62**	**$C41H^+$/C75**	**15**	**59 Na^+**
ProC41+C75+(1)	Product[b]	62	$C41H^+$/$C75H^+$	15	58 Na^+
ProC41+C75+(2)	Product[b]	62	$C41H^+$/$C75H^+$	11	58 Na^+
ProMgTrc	Product[b]	58[c]	C41/C75	16.5	38 Na^+ and 9 Mg^{2+}[d]
ProMg	Product[b]	62	C41/C75	8.2	42 Na^+ and 9 Mg^{2+}[d]
ProTrcC41+	Product[e]	58[c]	$C41H^+$/C75	15	55 Na^+

Simulations of unmodified crystal structures are shown in bold type.
[a] Precursor crystal structure, preliminarily refined version of PDB ID 1SJ3.[10]
[b] Self-cleaved product crystal structure, PDB ID, 1CX0.[9]
[c] In these simulations, the P4 stem was not extended by two additional G·C Watson–Crick base-pairs.
[d] Nine Mg cations placed initially as found in product crystal structure 1CX0.
[e] Started from 7.5 ns snapshot of simulation ProMgTrc.

Table 2. Hydrogen bonds found in the crystal structures of the product and precursor forms of the HDV ribozyme

			Distance (Å)	Angle (°)	Distance (Å)	Angle (°)
			Product		Precursor	
Clustered A-minor	A77(N3)	C19(HO′2)	2.5		2.7	
	A77(HO′2)	C19(O2′)	3.1		2.6	
	A78(HO′2)	C30(O2)	3.6		3.4	
	A78(N3)	G29(H22)	3.3	13.3	2.7	3.8
	A78(N1)	G29(HO′2)	2.7		2.6	
	A78(O2′)	C18(HO′2)	2.7		2.9	
	A78(HO′2)	C18(O2)	2.6		2.5	
J4/2 and the active site	C3(O1P)	U−1(H3)	–		2.8	50.5
	C/U75(H3)[a]	U−1(O3′)	–		3.5	32.3
	C/U75(H3)	G1(O1P)	–		2.6	71.4
	C/U75(O2)	G1(O5′H)	2.6		–	
	C/U75(N3)	G1(O5′H)	2.8		–	
	C/U75(H42)	U20(O2′)	2.8	56.8	–	
	C/U75(O2′)	C22(H42)	3.3	57.8	–	
L3 and P1.1	C/U75(H42)	C22(O2P)	3.0	28.9	–	
	C22(O2P)	U20(HO2′)	2.2		3.1	
	G25(O6)	U20(H3)	–	–	2.1	57.0
	C21(O2)	A42(H61)	2.9	32.2	2.7	34.8
J1.1/4 and P4	C21(HO′2)	A42(N1)	3.0		2.8	
	C21(O1P)	G74(HO′2)	2.5		2.5	
	G73(N7)	$C41H^+$(H41)	3.0	11.1	2.6	37.4
	G73(O6)	$C41H^+$(H3)	2.9	38.7	2.4	12.5
	G74(O6)	G40(H21,2)	2.5	34.7	2.7	43.2
	$C41H^+$(O2)	A43(H62)	2.8	58.1	3.1	22.9
	G40(N3)	A42(H62)	3.3	43.1	3.4	40.7
	G40(H22)	A42(N6)	3.3	32.4	3.3	24.5
	A42(N7)	G40(HO′2)	2.8		3.0	
	C44(O2)	G74(H21)	2.7	55.7	2.6	97.0

Distances between heavy-atoms are given in Å. Angles (in degrees) represent the deviation of the H-bond from linearity, that is (180°−A-H···B).

[a] U75 in the precursor structure and C75 in the product structure.

specific conformational substates of the simulated molecules will be discussed throughout the text while a full solvation analysis will be provided in a separate publication.

Joiner J4/2 and the catalytic pocket in the precursor simulations: a dynamic catalytic pocket allows for spontaneous formation of a transient U−1(O2′)-C75(N3) H-bond

The joiner J4/2 region contains nucleotides 75 through 78 between helices 2 and 4 (Figure 1(a)). In the precursor (as well as the product) these nucleotides fold into a "trefoil" turn in which G74, C75, and G76 form the three leaves of a clover, placing the 75 base deeply into the catalytic core of the ribozyme.[10] C75 is held in place by a network of H-bonds and by stacking interactions with A77. Insertion of the sugar edges of A77 and A78 into the minor groove of stem P3, forming a so-called A-minor motif,[48] further stabilizes the adjacent catalytic pocket (Figure 1(a)). All of these interactions help anchor C75 in the catalytic pocket.

The cleavage site G1 is engaged in a wobble pair with U37, forming the terminal base-pair of helix P1 (Figure 1(a)), which is stable in all our precursor and product simulations and involves a U37(O2), G1(N2) water bridge, in agreement with the known structure of such *cis*-Watson–Crick/Watson–Crick (*cis*-WC/WC) G·U base-pairs.[49] The sharp (∼180°) turn of the backbone about the scissile phosphate places the U−1 base in the precursor structure at the opening between the P1 stem and the L3 loop. In the crystal, the electron density for the U−1 base is weak. Consistent with this notion, our three precursor simulations show that the terminal unpaired nucleotide U−1 is very flexible, sampling several different H-bonds so that it never fully fits its crystallographic position. The base adopts several conformations, but typically U−1(O4) points in the direction of J1/2, which allows for free rotation around the U−1(O3′)-G1(P) bond (Figure 2).

Simulation PreC41+ with an unprotonated C75 results in a distinct structure of the catalytic pocket compared to the C75U mutant precursor and C75 wild-type product crystal structures (Figure 2(a)). No C22(O2P)-C75(N4) interaction occurs as observed in the product crystal structure; instead a C21(O2P)-C75(N4(-H42)) H-bond forms between ∼0.5 ns and 7.5 ns (Figure 2(a)). C75 generally fluctuates and is not as deeply lodged in the

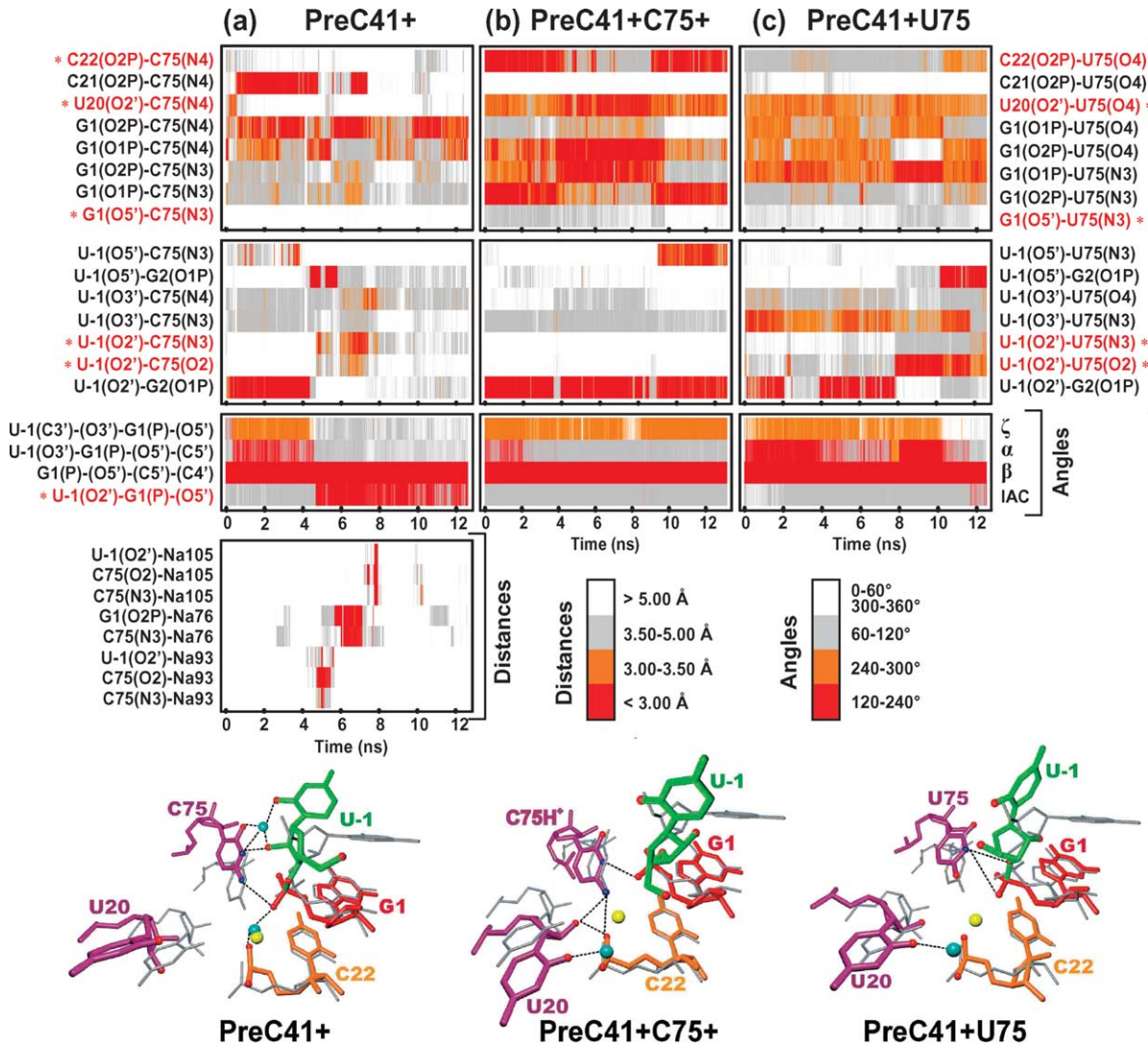

Figure 2. Structural dynamics of the catalytic pocket in precursor simulations (a) PreC41+, (b) PreC41+C75+ and (c) PreC41+U75. Time trajectories of heavy-atom distances and angles are shown over the entire simulation time (specific distances discussed in the text are highlighted in red and with a star). The same color scale for distance is used throughout the paper. Bottom panels: stick models showing an overlay of representative averaged structures of the catalytic pocket from our simulations (period 6.0–6.1 ns of simulation PreC41+, when the U−1(O2′)-C75(N3) H-bond is formed; period 6.9–7.0 ns of simulation PreC41+C75+; period 9.9–10.0 ns of simulation PreC41+U75; color-coded as for Figure 1(a); cyan spheres, Na ions; broken lines, H-bonds and inner-sphere ion contacts) with the precursor crystal structure (gray; yellow sphere, crystallographically resolved Mg ion).

catalytic pocket as in the two crystal structures and all our other simulations (Figures 1(d) and 2(a)).

Strikingly, among the spontaneous and transient H-bonds formed by the unprotonated C75 is the one between U−1(O2′) and C75(N3). This H-bond forms three times during the 13 ns of our simulation, of which the longest period with an occupancy of >85% lasts ∼1 ns (here and elsewhere we use the following H-bonding criteria: heavy-atom distance <3.4 Å and U−1(O2′)-U−1(H2′)···C75(N3) angle >100°) (Figure 2(a)). Such a H-bond needs to form initially for C75 to be able to act as the general base catalyst during site-specific self-cleavage.[10] We find that formation of this U−1(O2′)-C75(N3) H-bond in simulation PreC41+ is facilitated by the adjustment of the dihedral angles C3′-O3′-P-O5′ (ζ), O3′-P-O5′-C5′ (α), and P-O5′-C5′-C4′ (β) in the U−1-G1 backbone (Figure 2(a)).

In further support of a potential role of C75 as a general base, we find that the U−1(O2′)-G1(P)-(O5′) angle is ∼140° in simulation PreC41+ once the U−1(HO2′)-C75(N3) H-bond has formed (Figure 2(a)). The self-cleavage reaction mechanism requires an in-line attack configuration (IAC) where this U−1(O2′)-G1(P)-(O5′) angle approaches 180°, coupled with close proximity of U−1(O2′) and G1(P). Although catalysis itself of course cannot be described using classical MD, the fact that this angle is relatively close to 180° in simulation PreC41+ while it remains below 100° throughout simulation PreC41+C75+ (Figure 2(b)) suggests that an unprotonated C75 is more compatible with

formation of a suitable IAC than a protonated C75H$^+$. The U−1(O2′)-G1(P) distance fluctuates around 4 Å in both simulations PreC41+ and PreC41+C75+ (data not shown). Doudna and co-workers have proposed, based on the (static) precursor crystal structure, that the spontaneous formation of a geometrically optimized U−1(O2′)-C75(N3) H-bond may initiate backbone cleavage.[10]

The dynamics of the catalytic pocket in the PreC41+ simulation is coupled with Na$^+$ binding events that help establish the U−1(O2′)-C75(N3) H-bond. Over the time-course of the simulation (13 ns) three different cations in turn establish inner-shell contacts with C75(N3), making bridges with G1(O2P), U−1(O2′) or U−1(O2) (Figure 2(a), bottom). These sodium bridges are related to a major cation-binding site located at the catalytic pocket, which shows 100% inner-shell Na$^+$ occupancy. The U−1-G1 backbone rearrangement observed at ∼4.7 ns occurs simultaneously with the initial Na$^+$ bridge formation, and the presence of a U−1(O2′)-C75(N3) H-bond clearly coincides with the presence of an inner-shell bound Na ion (Figure 2(a)). In addition, the fluctuations in the G1(O2P)-C75(N3) and G1(O2P)-C75(N4) distances decrease significantly when the cation bridge is formed (Figure 2(a)). These observations are consistent with the notion that cation binding helps stabilize the C75 position with respect to G1 so that a H-bond between C75(N3) and U−1(2′OH) can be established, suggesting a possible structural role for cations in HDV ribozyme function. Our simulations are on the nanosecond timescale, however, providing only limited sampling. We thus cannot rule out that the U−1(O2′)-C75(N3) H-bond may occasionally form even without any cation close by. Conversely, the presence of divalent metal ions under experimental conditions, which are known to be more proficient than monovalents in promoting catalysis,[4] may amplify and/or modify the rearrangements in local architecture we observe. Nevertheless, our simulation PreC41+ reveals a dynamic behavior of the catalytically involved base C75 such that a U−1(O2′)-C75(N3) H-bond, a prerequisite for the general base catalysis model of C75, is rather readily formed.

Protonation of C75 in the precursor leads to stable binding of C75H$^+$ within the catalytic pocket without formation of a G1(O5′)-C75H$^+$(N3) H-bond

Protonation of C75 in precursor simulation PreC41+C75+ leads to a more stable H-bonding pattern of this base than observed for the unprotonated C75 in simulation PreC41+. The protonated C75H$^+$ is firmly bound by G1(O1P or O2P)-C75H$^+$(N3), C22(O2P)-C75H$^+$(N4(-H42)), and U20(O2′)-C75H$^+$(N4(-H42)) H-bonds (Figure 2(b)). For example, the U20(O2′)-C75H$^+$(N4(-H42)) H-bond is stable except for time periods 2–3.5 ns and 9.5–11 ns; however, even during this time its occupancy remains >60% (Figure 2(b)). Likewise, the C22(O2P)-C75H$^+$(N4(-H42)) H-bond is present except for the period ∼6.0–9.0 ns (Figure 2(b)). This stable binding of C75H$^+$ to C22 and U20 shifts C75H$^+$ towards L3, i.e. more deeply into the catalytic pocket, by ∼2.5 Å compared to simulation PreC41+ (compare Figure 2(a) and (b)). Notably, these structural dynamics of the active site resemble more those of the product rather than the precursor form (see also below). Our observations therefore show striking similarity to the conformational switch model by Doudna and co-workers, which proposes that C75, once protonated, shifts more deeply into the catalytic pocket as part of a larger conformational rearrangement that coincides with 5′ product departure.[10] Based on the comparison of the dynamics in the catalytic pocket of all our precursor simulations (see also PreC41+U75, below) we propose that the product-like binding of the 75 base requires the presence of both the N4 amino and N3-H3 imino groups. Our observations thus suggest that C75 protonation may play a more active role in the proposed conformational switch than previously thought.

The H-bonds formed by C75H$^+$ on our simulation timescale do not include one with G1(O5′) (Figure 2(b)), which would be a prerequisite for the alternative proposal that C75 acts as general acid catalyst protonating the 5′ oxygen leaving group of the reaction.[4] In fact, C75H$^+$ is stably bound quite far away from G1(O5′) (with a G1(O5′)-C75H$^+$(N3) distance >4 Å at all times; Figure 2(b)). Our MD simulations are thus less consistent with the structural model for C75H$^+$ that accompanies the general acid catalysis model of the HDV ribozyme, although we cannot rule out that a H-bond between G1(O5′) and C75H$^+$(N3) may form at longer timescales or in the presence of Mg cations. (Note, however, that our simulations are capable of significantly relocating nucleotide 75 within the catalytic pocket.) A third mechanistic proposal that is more compatible with our structural dynamics data is the notion that the protonated C75H$^+$, which we find extensively H-bonded to G1(O1P or O2P) (Figure 2(b)), promotes catalysis by electrostatically stabilizing the increased negative charge of the G1 phosphate group in the transition state (electrostatic catalysis).[50]

U75 in the precursor results in a less dynamic catalytic pocket, resembling the crystal structure

In simulation PreC41+U75, containing the original U75 of the mutant crystal structure, the U75 position and its H-bonding interactions with G1 and U−1 remain similar to those in the refined crystal structure, suggesting that our simulations indeed are a good approximation of the ribozyme's structural dynamics and, *vice versa*, that the crystal structure represents a high-occupancy (relatively low-energy) conformation. This also suggests that the larger dynamics observed for C75 in simulation PreC41+ is not due to the absence of the proximal,

crystallographically resolved Mg ion[10] from our precursor simulations. Our PreC41+U75 simulation shows dynamic switching between the two possible H-bonds, U−1(O3′)-U75(N3) (0–2 ns, 4.5–8 ns, and 10.5–12 ns) and G1(O1P)-U75(N3) (for the remainder of the simulation) (Figure 2(c)). The presence of such a dynamic bifurcated H-bond under crystallographic conditions may blur the electron density and perhaps explain the somewhat unusual position of U75 in the refined structure. Overall, the PreC41+U75 simulation is in good agreement with its corresponding crystal structure, while our simulations PreC41+ and PreC41+C75+ containing C75 and $C75H^+$, respectively, reveal more significant changes in conformation and H-bonding around the catalytic pocket.

Joiner J4/2 and the catalytic pocket in the product simulations: an unprotonated C75 is more stably bound than a protonated one

In the product crystal structure, C75 is held in place mainly by what appears to be a bifurcated G1(O5′)-C75(N3)/G1(O5′)-C75(O2) H-bond with G1 of the cleavage site, by a C22(O2P)-C75(N4) H-bond involving C22 in loop L3, and by stacking on the bottom face of A77 within J4/2 (Figure 3).[8,9] In our four product simulations with an unprotonated C75 (ProC41+, ProMgTrc, ProTrcC41+, ProMg), these H-bonds consistently remain quite stable (Figure 3(a)). Consequently, the position of C75 with respect to G1 is rather well defined with only minor fluctuations, suggesting that our simulations indeed are a good approximation of the ribozyme's structural behavior and, *vice versa*, that the crystal structure is a good approximation of a relatively low-energy conformation. By contrast, our two simulations with a protonated C75 (ProC41+C75+(1 and 2)) evolve in a way that the direct H-bond connecting G1 and C75 is disrupted and the two bases shift apart significantly, leading to the insertion of a water bridge between G1(O5′) and C75(N3) (Figure 3(b)). Our simulations thus support the notion that C75 is unprotonated in the product crystal structure, consistent with its observed acidic pK_a value of ∼4.8.[15]

Among the minor fluctuations in our four product simulations with unprotonated C75, the G1(O5′)-C75(N3) and G1(O5′)-C75(O2) H-bonds do not form a static bifurcated interaction but rather are best described as two distinct, dynamically competing (i.e. anticorrelated) H-bonds (Figure 3(a)). The alternate presence of these H-bonds is correlated with the depth of C75 penetration into the active site. Just a slight shift of C75 with respect to G1 (which itself is firmly bound by its G1·U37 wobble interaction) is required to switch between the two H-bonds, such that a deeper penetration of C75 leads to the G1(O5′)-C75(O2) H-bond, while a slight retraction leads to the G1(O5′)-C75(N3) H-bond or even, less frequently, a G1(O5′)-C75(N4(-H41)) H-bond instead (Figure 3(a)).

The C22(O2P)-C75(N4(-H42)) interaction of C75 with the L3 backbone, observed in the product crystal structure, is stable in most of our simulations with the following two exceptions. In simulations ProC41+C75+(1 and 2) a significant displacement of the protonated $C75H^+$ is observed (see above), which in simulation ProC41+C75+(1) leads to the slightly shifted C22(O2P)-C75(N4(-H41)) H-bond instead (Figure 3(b)) and in ProC41+C75+(2) results in complete disruption of the H-bond between 1.0 ns and 7.7 ns (Figure 3(a)). The U20(O2′)-C22(O2P) hydrogen bond was present with high occupancy in all simulations except ProTrcC41+ and ProMgTrc. The U20(O2′)-C75(N4(-H42)) and C22(N4(-H42))-C75(O2′) interactions observed in the product crystal structure were comparably unstable; they were disrupted or fluctuated with relatively low occupancy in all simulations including the "unmodified" (most crystal-structure like) ProC41+ simulation (Figure 3(a)). However, these temporary H-bond disruptions did not affect the general positioning of C75 (Figure 3(b)).

In summary, product simulations carried out with an unprotonated C75, especially the "unmodified" simulation ProC41+, are in good agreement with the crystal structure. Nevertheless, the C75 nucleobase exhibits modest dynamics within the catalytic pocket and its exact position is affected by adjacent parts of the ribozyme. Protonation of C75 is not compatible with the product crystal structure, as expected.[15]

Loop L3 is a dynamic structural element that controls the electrostatic environment of the catalytic pocket

L3 is an eight nucleotide loop closing the P3 stem (Figure 1). The helical stack of P3 is continued by the U20 and G25 bases, which stack on its terminal C19·G28 base-pair. C21 and C22 form the 3′ segment of P1.1. The crystal structures show evidence for high flexibility (i.e. a high *B* factor) of the L3 region, with the U23, C26 and U27 bases extruded from the helical stack and not well ordered (Figure 1(d)).[8,10] The precursor and product crystal structures differ significantly in the L3 region (Figure 4).[8,10] In all C75U precursor crystal structures, G25 is in the *anti* conformation forming a U20(N3)-G25(O6) H-bond. By contrast, in the product crystal structure G25 adopts a *syn* conformation such that U20 and G25 face each other with their Watson–Crick edges, yet the U20(O4)-G25(N1) and G25(O6)-U20(N3) distances of 5.2 Å and 4.2 Å, respectively, are too long for H-bonding (Figure 4(b)). Despite its apparent flexibility, L3 is relatively compact in all crystal structures so that an *anti*-to-*syn* interconversion of G25 from precursor to product would require at least a partial unfolding of L3. Interestingly, a G25A mutation that would stabilize standard Watson–Crick base-pairing with U20 reduces HDV ribozyme activity ∼3000-fold,[6] consistent with the notion that H-bonding between

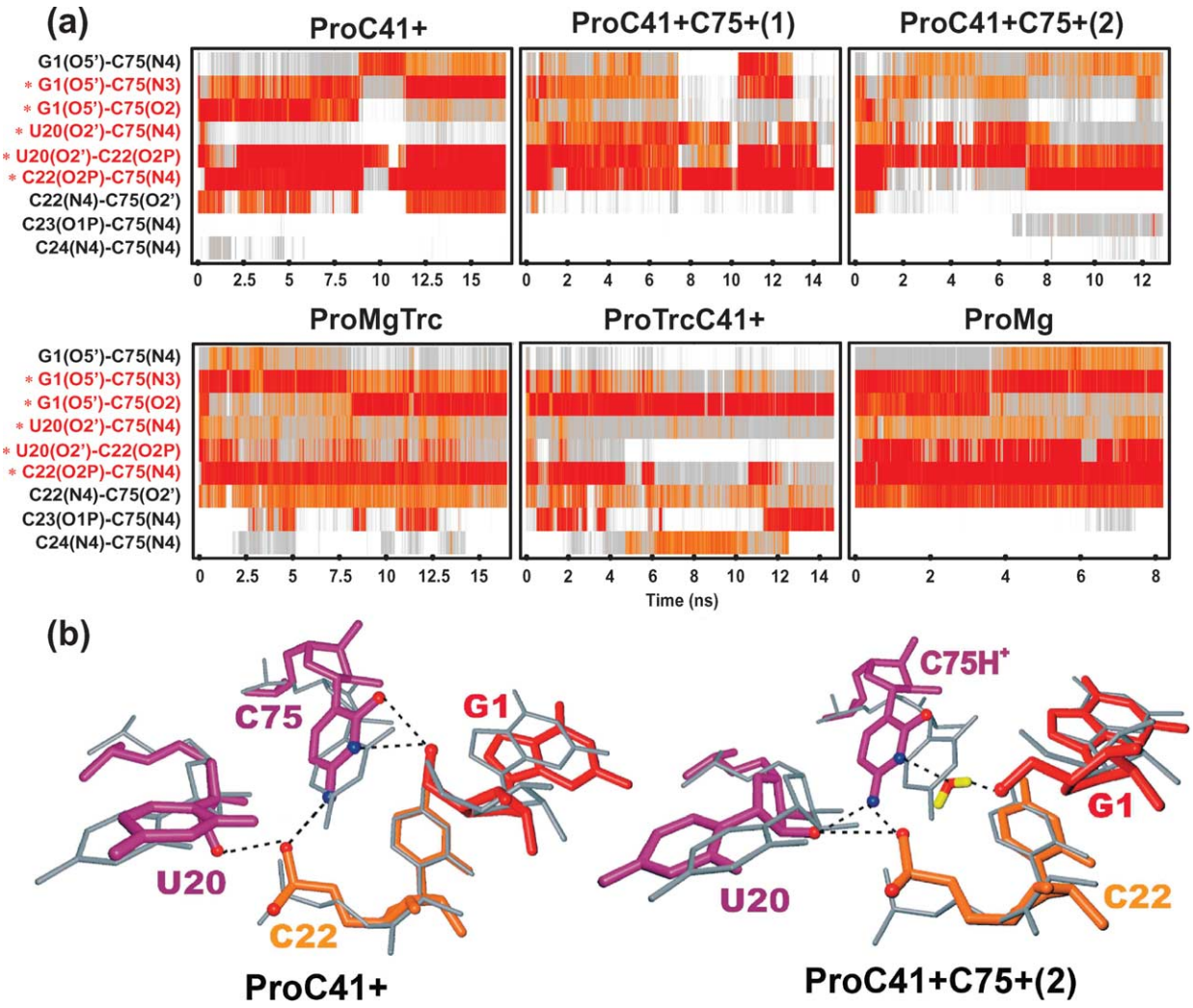

Figure 3. Structural dynamics of the catalytic pocket in our product simulations. (a) Time trajectories of heavy-atom distances shown over the entire simulation time (specific distances discussed in the text are highlighted in red and with a star). For the color scale see Figure 2. (b) Stick models showing an overlay of representative averaged structures of the catalytic pocket from our simulations (period 12.5–12.6 ns of simulation ProC41+; period 13.0–13.1 ns of simulation ProC41+C75+(1) including an inserted long-residency water molecule) with the product crystal structure (gray).

positions 20 and 25 must be sufficiently weak for catalysis to occur.

L3 retains its compact structure during most, but not all, of our precursor simulations, while different types of U20·G25 interactions are observed (Figure 4). For example, a *trans*-Watson–Crick/Hoogsteen base-pair with a direct U20(N3)-G25(N7) H-bond and a water bridge between U20(O2) and G25(O6) is found initially in simulation PreC41+ (Figure 4(a)). However, this *trans* base-pair is not stable and rearranges after ~1 ns into a *cis*-WC/WC "wobble" base-pair that remains stable until the end of the simulation (Figure 4(a) and (b)). By contrast, a similar *trans*-WC/WC base-pair with a single U20(N3)-G25(N7) H-bond is found throughout simulation PreC41+C75+ and up to 9 ns into simulation PreC41+U75 (Figure 4(a)). In both of these cases, the *trans* base-pair is stabilized by a long-residency Na^+ bridge between U20(O2) and G25(O6) (Figure 4(b)), the same position that is occupied by a water molecule in the first nanosecond of simulation PreC41+. Nine nanoseconds into simulation PreC41+U75, the ion suddenly departs and the U20·G25 *trans*-Watson–Crick/Hoogsteen base-pair is disrupted (Figure 4(a)), coinciding with partial unfolding of L3 in a way that may provide enough space for a G25 *anti*-to-*syn* rotation. It should be noted that the exact crystal orientation of U20·G25 is not preserved in any of our simulations, which is likely related to the lack of a Mg cation bound at L3.

In all product simulations, U20 and G25 form several different H-bonding arrangements, despite the fact that a base-pair is not fully formed in the initial crystal structure (Figure 4(a)). A *trans*-WC/WC base-pair with U20(O4)-G25(N1) and U20(N3)-G25(O6) H-bonds is stable throughout simulation ProC41+ and in the final stages of simulation ProC41+C75+(2) (Figure 4(a) and (b)). At the same time, loop L3 remains compact, rigid and similar to

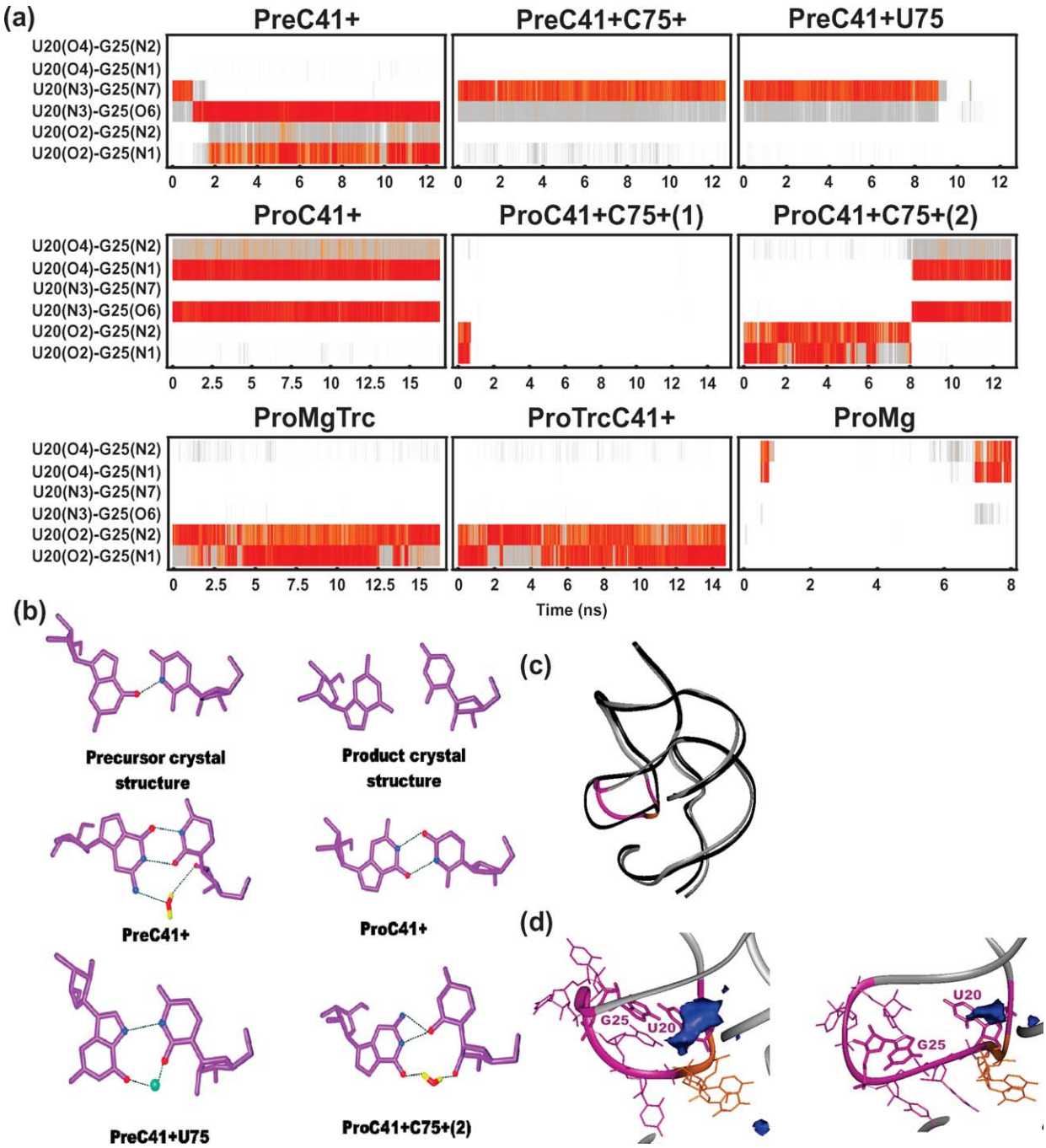

Figure 4. Structural dynamics of loop L3 during our MD simulations. (a) Time trajectories of heavy-atom distances for all observed H-bonds of the closing U20·G25 base-pair over the entire simulation time. For the color scale see Figure 2. (b) Six distinct geometries of the U20·G25 base-pair observed in the crystal structures and our simulations. (c) Overlay of the compact L3 architecture observed in the product crystal structure (silver and color) with the expanded architecture of L3 in simulation ProC41+C75+(1) (black; averaged over period 14.0–15.0 ns). (d) Negative electrostatic potential (NESP) map calculated for two averaged simulated structures and contoured at $-16\ kT/e$ (dark blue). Left, period 7.5–8.5 ns of simulation ProC41+ with compact L3 architecture; the deepest NESP minimum reaches $\sim -29\ kT/e$. Right, period 14.0–15.0 ns of simulation ProC41+C75+(1) with expanded L3 architecture; the deepest NESP minimum reaches only $\sim -21\ kT/e$.

the crystal structure, except for a minor shift towards the center of the structure due to completion of the U20·G25 base-pair.

In simulations ProMgTrc, ProTrcC41+, and the initial parts of ProC41+C75+(1) and ProC41+C75+(2), a fluctuating base-pair occurs that involves U20(O2)-G25(N1) and U20(O2)-G25(N2 (-H21)) H-bonds (Figure 4(a) and (b)). This base-pair becomes completely disrupted 1 ns into simulation ProC41+C75+(1) (Figure 4(a)). This disruption leads to subsequent disappearance of L3 bending near G25, resulting in a marked

elongation of the loop (Figure 4(c)). L3 becomes very flexible and samples a large conformational space during which G25 stacks on U27 ~90% of the time, blocking any *syn*-to-*anti* interconversion. U20 remains stacked on the terminal C19·G28 base-pair of P3. After 4.5 ns, L3 shifts closer to J1.1/4 and establishes C24(N4(-H41))-A42(N3) and G23(N3)-A42(N1) H-bonds (yet no interactions with other parts of the RNA), leading to visible fluctuations in J1.1/4 (data not shown). However, such an open geometry of L3 is not observed in the parallel simulation ProC41+C75+(2), except for a modest fluctuation in its initial part. Thus, large-scale L3 unfolding and subsequent G25 *anti-syn* interconversions may be relatively rare events and we cannot estimate their statistical significance based on our simulation timescale. Nevertheless, an expanded architecture clearly represents a plausible substate within the conformational space of L3.

We thus find that U20 and G25 establish a number of very dynamic H-bonding interactions whose interconversion may serve as a structural trigger for L3 unfolding. The behavior of our simulations PreC41+U75, ProC41+C75+(1), and ProMg may then represent some possible initial paths for such L3 unfolding. L3 is connected with the rest of the RNA through a number of H-bonds to C75 and adjacent residues (such as U20(O2′)-C75(N4(-H41)), C22(O2P)-C75(N4(-H42)) (Figure 2), C21(O2)-A42(H61), and C21(O1P)-G74(O2′)), suggesting that changes in L3 may propagate into the catalytic core. However, in our simulations L3 dynamics leads only to the mostly local fluctuations of H-bonds discussed above (Figure 4(c)).

A more indirect way of communication between loop L3 and the catalytic core may derive from the fact that L3 is a strong determinant of the electrostatic environment of the catalytic pocket. The HDV ribozyme as a compact RNA molecule exhibits several strong negative electrostatic potential (NESP) sites. The deepest NESP region in the HDV ribozyme covers loop L3 and the catalytic pocket (Figure 4(d)). This NESP region in the active site is significantly (on average by ~20 kT/e) deeper in the PreC41+ precursor simulation than it is in the ProC41+ product simulation due to the additional presence of the G1 phosphate and the U−1 nucleotide (see Figure 6(b), below). It also may help attract cations to the active site to bind near the scissile phosphate as observed in the precursor, but not the product crystal structure.[9,10] Consistent with this notion, our simulations PreC41+, PreC41+C75+ and PreC41+U75 attract Na ions into this NESP minimum, as described above. This long-residency cation-binding site is seen in all simulations carried out without Mg cations and coincides strikingly with the Mg^{2+} position observed in the precursor crystal structure (Figures 2 and 4).

The effect of loop L3 on the active site NESP is most noticeable in our product simulation ProC41+C75+(1). Figure 4(d) shows representative NESP maps (of the active site and L3) calculated for averaged structures from simulations ProC41+ and ProC41+C75+(1) with the compact and expanded L3 architectures, respectively. The expansion of L3 markedly decreases the NESP site of the catalytic pocket in both width and depth compared to the compact L3 architecture in simulation ProC41+. To control for the contribution of the positive charge of $C75H^+$, the NESP map was also calculated for early on in the ProC41+C75+(1) simulation (averaged over 0.5–1.0 ns), when L3 is still compact, which resulted in a map very similar to the one shown on the left side of Figure 4(d) for the unprotonated ProC41+. Furthermore, a similarly specific effect of L3 unfolding on NESP maps was observed for structures from simulation PreC41+U75 with compact and unfolded L3 (data not shown). Our simulations thus support the notion that the electrostatic environment of C75 is strongly affected by the adjacent L3 architecture.

The J1.1/4 junction unfolds in the absence of C41 protonation

Joiner J1.1/4 is a three nucleotide turn-like junction between the P1.1 and P4 stems.[8,10] The arrangements of P4 and J1.1/4 are identical in the product and precursor crystal structures (Figure 1(a) and (b)).[8,10] The most prominent feature of joiner J1.1/4 is base C41, which is in H-bonding contacts that suggest it is protonated in the crystal structures at pH values as high as pH 7.0[8] to form an $A_{(n-1)}\cdot C^+\cdot G\cdot C_{-n}$ quadruple, a recurring RNA motif.[51] In this quadruple between A43, $C41H^+$, G73 and C44 (Figure 1(a)), $C41H^+$ forms $C41H^+$(N4(-H41))-G73(N7), $C41H^+$(N3)-G73(O6), and $C41H^+$(O2)-A43(N6(-H62)) H-bonds, which are stable in all our simulations where C41 is protonated (Figure 5(a)). In simulations ProMgTrc and ProMg, where C41 is unprotonated, the *trans*-Watson–Crick/Hoogsteen $C41(H^+)\cdot G73$ base-pair and the compact arrangement of J1.1/4 are rapidly disrupted (Figure 5(a) and (b)). A Na cation (for ~1.1 ns during simulation ProMgTrc and almost until the end of simulation ProMg) appears to substitute for the missing C41(N3) proton by forming a sodium bridge to G73(O6) of stem P4 (Figure 5(b)). Although this Na^+ insertion somewhat preserves the overall J1.1/4-P4 architecture, it still leads to a significant increase in the distance between the Watson–Crick face of C41 and the Hoogsteen face of G73 and thus to the loss of their H-bonding interactions (Figure 5(b)). About 2 ns into simulation ProMgTrc the whole J1.1/4 region unfolds as evident from multiple local structural changes and H-bond losses (Figure 5(a)). This leads to a new H-bonding network that persists until the end of the simulation and is markedly different from that of the crystal structure (Figure 5(b)). When J1.1/4 unfolds in this fashion, the P4 stem bends due to local changes of the J1.1/4-P4 region, involving an increase of the C21|G74 slide by ~1.5 Å and a decrease in tilt and twist between the C44·G73 and A43·G74 base-pairs by ~12° and

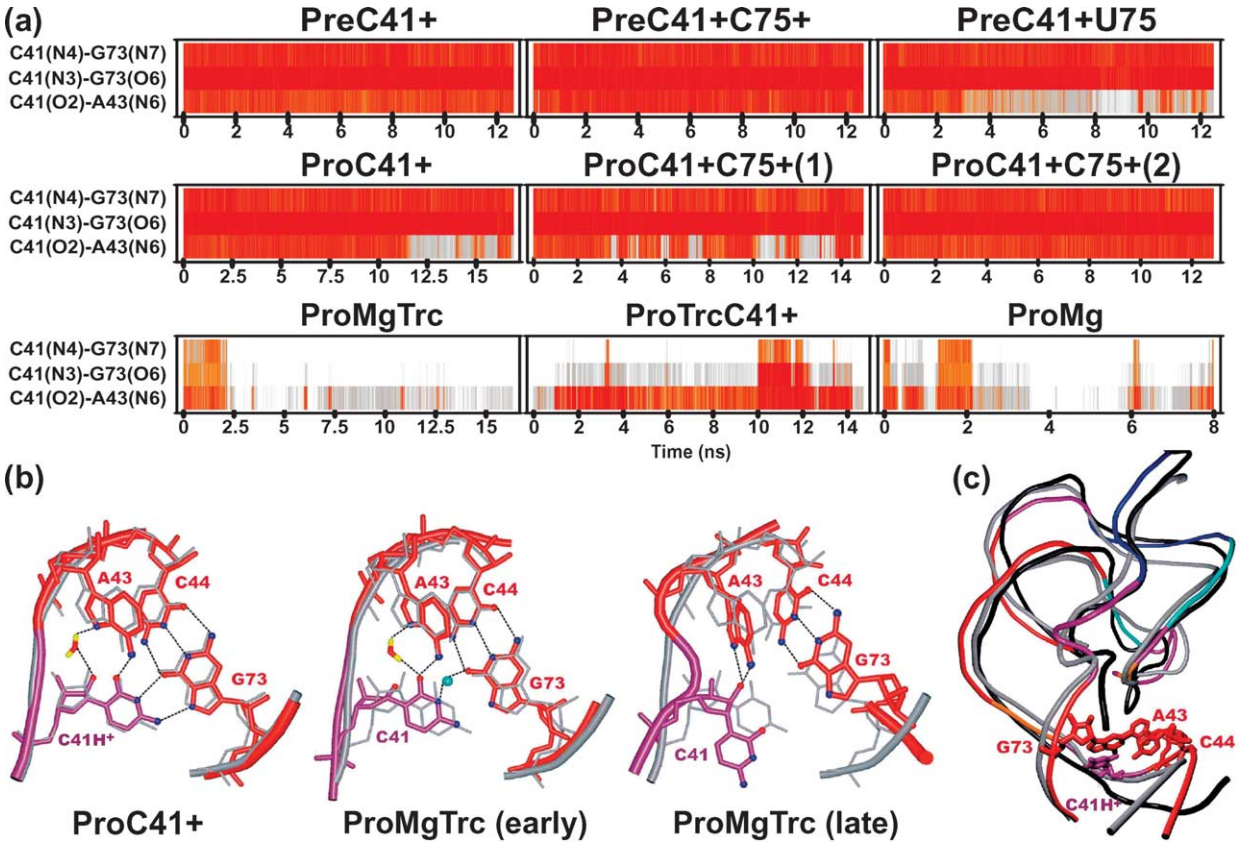

Figure 5. Structural dynamics of the A43·C41H$^+$·G73·C44 quadruple. (a) Time trajectories of heavy-atom distances for all H-bonds of C41 over the entire simulation time. For the color scale see Figure 2. (b) Structural effect of the loss of C41 protonation in comparison to the product crystal structure (gray). Left, averaged structure from simulation ProC41+ (color), including a long-residency water molecule. Middle, averaged structure from early in simulation ProMgTrc (color), showing evidence for initial stabilization of the base quadruple *via* Na ion insertion (cyan). Right, averaged structure from late in simulation ProMgTrc (color), showing that the base quadruple is completely lost. (c) Overlay of the complete backbone of the product crystal structure (gray) with those of the averaged structures from simulations ProC41+ (color) and late in simulation ProMgTrc (black), with the base quadruple indicated.

25°, respectively. As a consequence, the direction of the P4 stem is changed so that it is no longer collinear with P1.1 (Figure 5(c)). (The changes were considerably smaller in simulation ProMg, since the compensating Na cation was bound until 8.2 ns into the 8.4 ns long simulation.) When C41 is re-protonated after the J1.1/4 unfolding (simulation ProTrcC41+; Table 1), the original C41H$^+$·G73 H-bonds are temporarily formed between ~10 ns and ~12 ns (Figure 5(a)), but only at the expense of partial disruption of the C44·G73 Watson–Crick base-pair in stem P4 (data not shown). A disrupted J1.1/4-P4 structure thus is not repaired on our simulation timescale.

In summary, we find that the quadruple interaction in J1.1/4 depends critically on protonation of C41. In the presence of a protonated C41H$^+$J1.1/4 fluctuations are generally small, while the intricate J1.1/4 structure quickly becomes instable when C41 is unprotonated. A protonated C41H$^+$ thus helps firmly connect P1.1 with P4 through J1.1/4 in a collinear arrangement. Although J1.1/4 is not close enough to be typically viewed as part of the catalytic core of the HDV ribozyme, it is intriguing to note that its stacking partner P1.1 itself stacks under the cleavage site G1·U37 wobble pair, while C41 and G40 make H-bonds with G73 and G74, adjacent to C75. It therefore appears plausible that unfolding of J1.1/4 in the absence of C41 protonation may lead to detrimental conformational rearrangements in the catalytic core (which are not observed here, most likely due to our limited simulation timescale). Notably, we find a Na ion to partially and temporarily compensate for the loss of the protonated H-bond by forming a Na ion bridge in its place. This is surprisingly consistent with the experimentally observed synergy between low pH and high Na$^+$ concentrations in mediating residual self-cleavage of the genomic HDV ribozyme in the absence of divalents.[11]

Conclusions

The HDV ribozyme was the first RNA enzyme for which structural and mechanistic evidence supported the idea that it utilizes one of its own nucleobases, rather than an external ligand such

as a hydrated Mg ion, for general acid/base catalysis.[3,4,8,10] While subsequent proposals have suggested that this catalytic strategy may also be employed by the ribosome[52,53] and the hairpin ribozyme,[54,55] evidence in these cases has been more controversial.[56–63] This makes the HDV ribozyme currently the prime model for an RNA with a specific side-chain (C75) that directly participates in chemical catalysis.[50]

While the notion that C75 participates in catalysis is uncontroversial, its exact role, as either general base or general acid, is much less clear due to the inherent ambiguity of mechanistic studies.[3,4,11–14,50] Both mechanistic models are associated with distinct proposals for conformational rearrangements necessary to allow for subsequent catalysis. To provide for an approach to assess the structural dynamics of the enzyme and bridge the gap between X-ray crystallography, which reveals atomistic, yet static structural information, and mechanistic studies, which probe the structural dynamics of an enzyme on a global scale, we have turned to molecular dynamics simulations in explicit solvent. In particular, we find that: (i) simulations based on the unmodified crystal structures remain relatively close to their respective input structures, indicating that the simulations are relatively conservative. (ii) An unprotonated C75 shows comparably weak hydrogen bonding interactions in the catalytic pocket of the precursor, which include a transient H-bond between C75(N3) and U−1(O2′); formation of this H-bond accompanied by other conformational rearrangements is a prerequisite for mechanistic models that invoke C75 as the general base (Figure 6(a)). (iii) When protonated in the precursor, $C75H^+$ moves towards its product location and establishes a stable H-bonding network within the catalytic pocket; this does not include, however, a $C75H^+$(N3)-G1(O5′) H-bond that is the structural prerequisite for general acid models of C75 catalysis; instead, a H-bond with one of the non-bridging phosphate oxygen atoms of G1 is formed, which could later help to electrostatically stabilize this phosphate's increased negative charge in the transition state of the reaction (Figure 6(a)); taken together, these observed structural dynamics are most compatible with the general base catalysis model for C75 (Figure 6(a)). (iv) Loop L3 occasionally unfolds, triggered by dynamic changes in its closing U20·G25 base-pair; L3 strongly determines the negative electrostatic potential of the catalytic pocket; and the electrostatic potential minimum in the catalytic pocket is considerably deeper for the precursor than the product structure due to the additional presence of the G1 phosphate and differences in L3 conformation (Figure 6(b)); NESP changes in turn may modulate C75 base strength as well as binding of a metal ion as a possible structural and/or chemical participant of catalysis. (v) The structural integrity of a quadruple interaction in J1.1/4 depends critically on protonation of C41; this quadruple maintains a collinear arrangement between P1.1 and P4, which when lost may lead to detrimental conformational rearrangements in the catalytic core; a Na ion transiently compensates for the lack of a protonated H-bond of C41 by forming a Na ion bridge instead; this finding is surprisingly consistent with the experimental observation that a low pH combined with a high Na^+ concentration leads to residual self-cleavage of HDV ribozymes containing the J1.1/4 quadruple.[11]

When evaluating the present results, it is important to note that the outcome of simulations is affected by approximations and limitations. First, approximations originate from the use of simple pair-additive analytic empirical potential functions. However, the Cornell *et al.* force field is thought to provide a balanced description of base stacking and H-bonding, superior to other force fields.[64] Additional care needs to be taken regarding the backbone description. The backbone is described by a set of simple torsional functions and its behavior may be further affected by the use of conformation-independent atom-centered electrostatic-potential derived point charges. While such a charge model is entirely sufficient for base stacking and H-bonding of rigid nucleobases, its application to a flexible and anionic backbone chain is less realistic, as constant charges cannot fully describe the changes in electrostatic potential in response to changes in geometry. In fact, accumulation of long-lived backbone flips was recently reported in extended *B*-DNA simulations.[46] We thus monitored the behavior of the backbone dihedral angles very carefully and concluded that no unusual or excessive backbone flips occurred in our present or preceding simulations of various RNA molecules.[33,34,40,65] This suggests that RNA simulations, at least on the current state-of-the-art timescale, are well behaved. In fact, the backbone torsional angles at the end of our simulations appear to be more regular (when comparing with established RNA backbone conformational families[66]) than the backbone geometries in the starting, medium-resolution crystal structures.

Second, a potential limitation is the current nanosecond-scale of simulations that prevents the crossing of more substantial free energy barriers. We wish to underline that the motion of the 75 base in the catalytic pocket does not appear to be hindered by significant energy barriers and should be relatively well sampled. Yet, our simulations are certainly not sufficiently long to achieve a representative sampling of, for example, the very flexible L3 region. A specific problem is presented by Mg cations that are poorly represented by simple force fields (as major polarization and charge transfer effects are neglected). As shown recently,[65] improperly placed Mg^{2+} can cause substantial perturbations of a simulated RNA structure, which are not repaired in the course of the simulation. For this reason, the present analysis was primarily based on simulations utilizing monovalent cations that are better described by the force field and show sufficient sampling.[33,34,39,46,65]

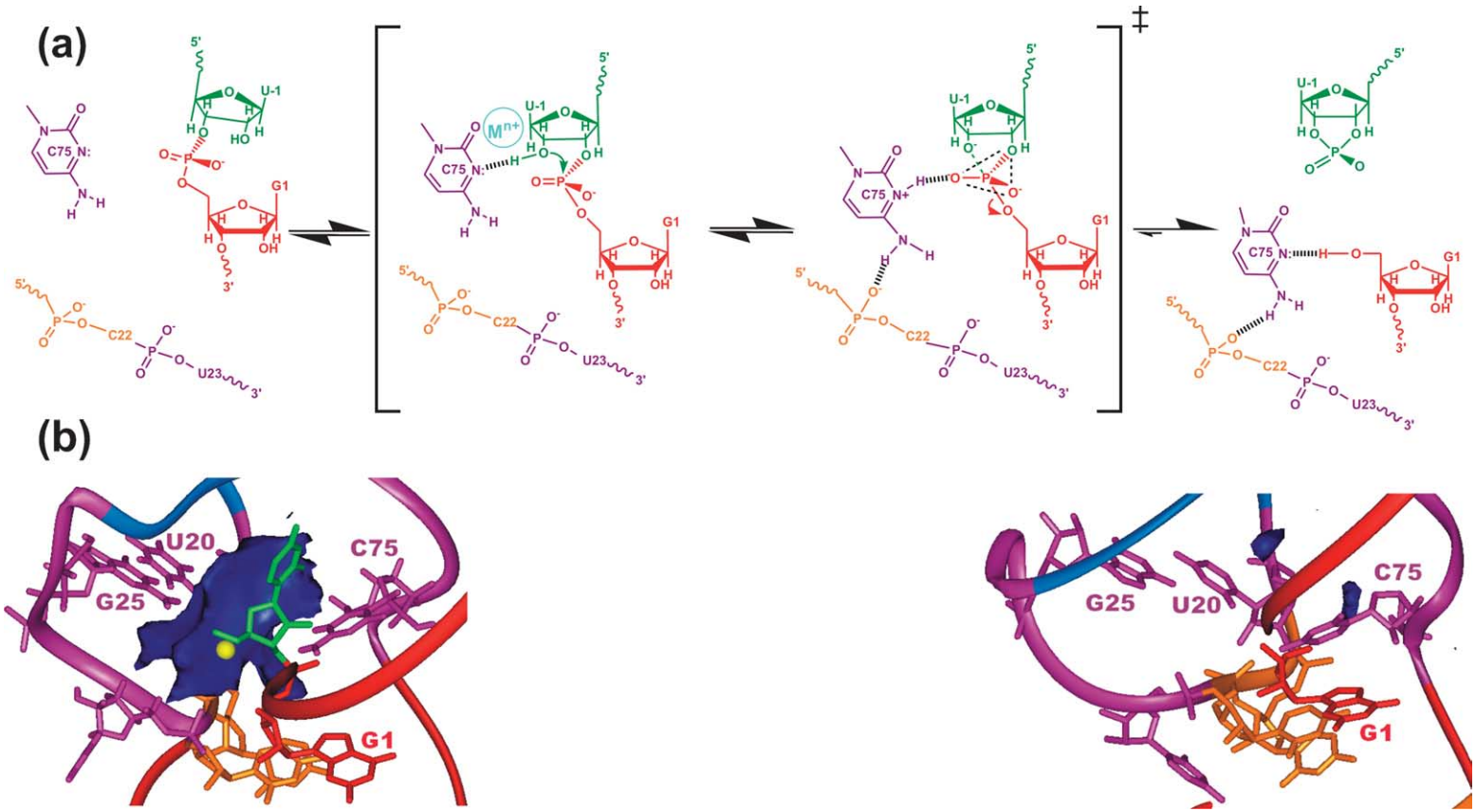

Figure 6. (a) Model of the cleavage reaction mechanism of the HDV ribozyme, involving general base catalysis by C75 (color-coded as for Figure 1(a)). The ground states before and after cleavage are described by the precursor and product crystal structures, respectively, with observed H-bonds indicated by broken lines. The transition state is characterized by successive conformational changes involving H-bond formation between C75(N3) and U−1(O2′) (middle left), as observed in our simulation PreC41+, and following H-bond formation between a protonated C75H$^+$(N3) and a non-bridging oxygen atom of the G1 phosphate group and between C75H$^+$(N4) and C22(O2P) (middle right), as observed in our simulation PreC41+C75+. (b) NESP maps of the precursor (left) and product crystal structures (right), contoured at $-20\ kT/e$ (dark blue); yellow sphere, Mg ion.

When assessing RNA simulations, the reader should keep in mind the potential limitations described above. Our findings nevertheless suggest that MD simulations, when used prudently, represent a valuable tool to assess qualitatively the structural dynamics leading to conformational substates appropriate for RNA catalysis. MD simulations thus provide guidance for future experimental studies and complement the static pictures obtained by X-ray crystallography. Finally, they pave the way for the application of advanced quantum chemical tools to probe more deeply into the reaction mechanism of catalytic RNAs.

Materials and Methods

Initial structures

Our simulations started from the crystal structures of the precursor[10] and 3′ product[9] forms of the HDV ribozyme. The structure of the catalytically inactive C75U mutant precursor (PDB ID, 1SJ3; 2.20 Å resolution) was modified using InsightII to carry C75 of the wild-type. (We used a preliminary structure in most of our simulations that was available several months ahead of publication, but did not contain a fully refined U−1. It differs slightly from the final refined structure in its U−1-G1 backbone arrangement (see also below). In addition, U−1 is bound to the P1 stem by a U−1(O4)-C4(N4(-H42)) H-bond, making for a very short U−1(N3)-C3(N4) contact of 1.89 Å. This small perturbation of the very dynamic U−1 does not have any significant effect on our simulations, since a 3 ns control simulation starting from the fully refined structure yielded very similar dynamics (data not shown).) Our modeling of the wild-type C75 into the mutant structure is validated by the fact that the lower-resolution crystal structure of a wild-type precursor in the absence of divalents (PDB ID, 1VC5; 3.4 Å resolution) has essentially the same structure as the C75U mutant (RMSD value of 0.30 Å).[10] The 3′ product crystal structure (PDB ID, 1CX0; 2.3 Å resolution) was used directly.[9] In both cases the unessential P4 stem, modified during crystallization to bind U1A protein, was truncated to facilitate computation (Figure 1(a)).

Molecular dynamics

All MD simulations were carried out using the AMBER7.0 program package[67] with the parm99 Cornell *et al.* force field.[68–70] The RNA was solvated in a rectangular box of TIP3P water molecules[71] extended to a distance of $\geq$10 Å from any solute atom. Mg cations (when present) were taken from the experimental PDB map. The simulated system was neutralized by sodium cations[72] initially placed by the LeaP module at points of favorable electrostatic potential close to the RNA. This corresponds to an ion concentration of $\sim$0.2 M. The Sander module of AMBER7.0 was used for the equilibration and production simulations using standard protocols (see, e.g. Spackova *et al.*[73]). The particle mesh Ewald method[74] was applied with a heuristic pair list update, using a 2.0 Å non-bonded pair list buffer and a 9.0 Å cutoff. A charge grid spacing of close to 1 Å and a cubic interpolation scheme were used. The production runs were carried out at 300 K with constant-pressure boundary conditions using the Berendsen temperature coupling algorithm[75] with a time constant of 1.0 ps. SHAKE[76] was applied in the simulations with a tolerance of 10^{-8} to constrain bonds involving hydrogen atoms.

Analysis of MD trajectories

The trajectories were analyzed using the carnal and ptraj modules of the AMBER7.0 package and our own scripts. The structures were visualized using the programs VMD[77] and InsightII (Accelrys, Inc.). RMSD values of individual nucleotides with respect to their positions in the crystal structure were obtained using the carnal module for each nucleotide without considering hydrogen atoms. Time trajectories of heavy-atom distances and angles were represented as list density plots using the program Mathematica 4.0. Electrostatic potentials were calculated using the program CMIP[78] by solving the non-linear Poisson–Boltzmann equation for ionic strength 0.2 M. Each atom was placed in a medium with a dielectric constant of 2 in the solvent-inaccessible surface-enclosed volume, which was obtained using a probe radius of 1.4 Å, while solvent was treated as a continuum with a dielectric constant of 80.

Acknowledgements

This work was supported by grants GA203/05/0009, Grant Agency of the Czech Republic, research project AVOZ50040507, Ministry of Education of the Czech Republic (Institute of Biophysics) and Wellcome Trust International Senior Research Fellowship in Biomedical Science in Central Europe GR067507 (to J.Š.); by NIH grant GM62357 including supplement S2 for acquisition of a computer cluster (to N.G.W.); and by a Margaret and Herman Sokol International Summer Research Fellowship, a NATO Science Fellowship, a Center for the Education of Women Sarah Winans Newman Scholarship, and an Eli Lilly Fellowship (to J.Š.). We are grateful to Drs Jennifer Doudna and Ailong Ke for making the coordinates of their precursor crystal structures available prior to publication. All simulations were carried out at the National Center for Biomolecular Research and the Supercomputer Center in Brno.

Supplementary Data

Supplementary data associated with this article can be found, in the online version, at doi:10.1016/j.jmb.2005.06.016

References

1. Lai, M. M. (1995). The molecular biology of hepatitis delta virus. *Annu. Rev. Biochem.* **64**, 259–286.
2. Shih, I. H. & Been, M. D. (2002). Catalytic strategies of the hepatitis delta virus ribozymes. *Annu. Rev. Biochem.* **71**, 887–917.

3. Perrotta, A. T., Shih, I. & Been, M. D. (1999). Imidazole rescue of a cytosine mutation in a self-cleaving ribozyme. *Science*, **286**, 123–126.
4. Nakano, S., Chadalavada, D. M. & Bevilacqua, P. C. (2000). General acid-base catalysis in the mechanism of a hepatitis delta virus ribozyme. *Science*, **287**, 1493–1497.
5. Kumar, P. K., Suh, Y. A., Miyashiro, H., Nishikawa, F., Kawakami, J., Taira, K. & Nishikawa, S. (1992). Random mutations to evaluate the role of bases at two important single-stranded regions of genomic HDV ribozyme. *Nucl. Acids Res.* **20**, 3919–3924.
6. Tanner, N. K., Schaff, S., Thill, G., Petit-Koskas, E., Crain-Denoyelle, A. M. & Westhof, E. (1994). A three-dimensional model of hepatitis delta virus ribozyme based on biochemical and mutational analyses. *Curr. Biol.* **4**, 488–498.
7. Perrotta, A. T. & Been, M. D. (1996). Core sequences and a cleavage site wobble pair required for HDV antigenomic ribozyme self-cleavage. *Nucl. Acids Res.* **24**, 1314–1321.
8. Ferre-D'Amare, A. R., Zhou, K. & Doudna, J. A. (1998). Crystal structure of a hepatitis delta virus ribozyme. *Nature*, **395**, 567–574.
9. Ferre-D'Amare, A. R. & Doudna, J. A. (2000). Crystallization and structure determination of a hepatitis delta virus ribozyme: use of the RNA-binding protein U1A as a crystallization module. *J. Mol. Biol.* **295**, 541–556.
10. Ke, A., Zhou, K., Ding, F., Cate, J. H. & Doudna, J. A. (2004). A conformational switch controls hepatitis delta virus ribozyme catalysis. *Nature*, **429**, 201–205.
11. Wadkins, T. S., Shih, I., Perrotta, A. T. & Been, M. D. (2001). A pH-sensitive RNA tertiary interaction affects self-cleavage activity of the HDV ribozymes in the absence of added divalent metal ion. *J. Mol. Biol.* **305**, 1045–1055.
12. Shih, I. H. & Been, M. D. (2001). Involvement of a cytosine side chain in proton transfer in the rate-determining step of ribozyme self-cleavage. *Proc. Natl Acad. Sci. USA*, **98**, 1489–1494.
13. Nakano, S. & Bevilacqua, P. C. (2001). Proton inventory of the genomic HDV ribozyme in Mg(2+)-containing solutions. *J. Am. Chem. Soc.* **123**, 11333–11334.
14. Oyelere, A. K., Kardon, J. R. & Strobel, S. A. (2002). pK(a) perturbation in genomic Hepatitis Delta Virus ribozyme catalysis evidenced by nucleotide analogue interference mapping. *Biochemistry*, **41**, 3667–3675.
15. Luptak, A., Ferre-D'Amare, A. R., Zhou, K., Zilm, K. W. & Doudna, J. A. (2001). Direct pK(a) measurement of the active-site cytosine in a genomic hepatitis delta virus ribozyme. *J. Am. Chem. Soc.* **123**, 8447–8452.
16. Pereira, M. J., Harris, D. A., Rueda, D. & Walter, N. G. (2002). Reaction pathway of the trans-acting hepatitis delta virus ribozyme: a conformational change accompanies catalysis. *Biochemistry*, **41**, 730–740.
17. Harris, D. A., Rueda, D. & Walter, N. G. (2002). Local conformational changes in the catalytic core of the trans-acting hepatitis delta virus ribozyme accompany catalysis. *Biochemistry*, **41**, 12051–12061.
18. Jeong, S., Sefcikova, J., Tinsley, R. A., Rueda, D. & Walter, N. G. (2003). Trans-acting hepatitis delta virus ribozyme: catalytic core and global structure are dependent on the 5′ substrate sequence. *Biochemistry*, **42**, 7727–7740.
19. Tinsley, R. A., Harris, D. A. & Walter, N. G. (2003). Significant kinetic solvent isotope effects in folding of the catalytic RNA from the hepatitis delta virus. *J. Am. Chem. Soc.* **125**, 13972–13973.
20. Tinsley, R. A., Harris, D. A. & Walter, N. G. (2004). Magnesium dependence of the amplified conformational switch in the trans-acting hepatitis delta virus ribozyme. *Biochemistry*, **43**, 8935–8945.
21. Harris, D. A., Tinsley, R. A. & Walter, N. G. (2004). Terbium-mediated footprinting probes a catalytic conformational switch in the antigenomic hepatitis delta virus ribozyme. *J. Mol. Biol.* **341**, 389–403.
22. Tanaka, Y., Tagaya, M., Hori, T., Sakamoto, T., Kurihara, Y., Katahira, M. & Uesugi, S. (2002). Cleavage reaction of HDV ribozymes in the presence of Mg^{2+} is accompanied by a conformational change. *Genes Cells*, **7**, 567–579.
23. Perrotta, A. T. & Been, M. D. (1990). The self-cleaving domain from the genomic RNA of hepatitis delta virus: sequence requirements and the effects of denaturant. *Nucl. Acids Res.* **18**, 6821–6827.
24. Auffinger, P. & Westhof, E. (1998). Simulations of the molecular dynamics of nucleic acids. *Curr. Opin. Struct. Biol.* **8**, 227–236.
25. Auffinger, P., Louise-May, S. & Westhof, E. (1999). Molecular dynamics simulations of solvated yeast tRNA(Asp). *Biophys. J.* **76**, 50–64.
26. Nagan, M. C., Beuning, P., Musier-Forsyth, K. & Cramer, C. J. (2000). Importance of discriminator base stacking interactions: molecular dynamics analysis of A73 microhelix(Ala) variants. *Nucl. Acids Res.* **28**, 2527–2534.
27. Sarzynska, J., Kulinski, T. & Nilsson, L. (2000). Conformational dynamics of a 5S rRNA hairpin domain containing loop D and a single nucleotide bulge. *Biophys. J.* **79**, 1213–1227.
28. Cheatham, T. E., 3rd & Young, M. A. (2000). Molecular dynamics simulation of nucleic acids: successes, limitations, and promise. *Biopolymers*, **56**, 232–256.
29. Blakaj, D. M., McConnell, K. J., Beveridge, D. L. & Baranger, A. M. (2001). Molecular dynamics and thermodynamics of protein-RNA interactions: mutation of a conserved aromatic residue modifies stacking interactions and structural adaptation in the U1A-stem loop 2 RNA complex. *J. Am. Chem. Soc.* **123**, 2548–2551.
30. Csaszar, K., Spackova, N., Stefl, R., Sponer, J. & Leontis, N. B. (2001). Molecular dynamics of the frame-shifting pseudoknot from beet western yellows virus: the role of non-Watson–Crick base-pairing, ordered hydration, cation binding and base mutations on stability and unfolding. *J. Mol. Biol.* **313**, 1073–1091.
31. Schneider, C., Brandl, M. & Suhnel, J. (2001). Molecular dynamics simulation reveals conformational switching of water-mediated uracil-cytosine base-pairs in an RNA duplex. *J. Mol. Biol.* **305**, 659–667.
32. Pitici, F., Beveridge, D. L. & Baranger, A. M. (2002). Molecular dynamics simulation studies of induced fit and conformational capture in U1A-RNA binding: do molecular substates code for specificity? *Biopolymers*, **65**, 424–435.
33. Reblova, K., Spackova, N., Stefl, R., Csaszar, K., Koca, J., Leontis, N. B. & Sponer, J. (2003). Non-Watson–Crick base-pairing and hydration in RNA motifs: molecular dynamics of 5S rRNA loop E. *Biophys. J.* **84**, 3564–3582.
34. Reblova, K., Spackova, N., Sponer, J. E., Koca, J. & Sponer, J. (2003). Molecular dynamics simulations of

RNA kissing-loop motifs reveal structural dynamics and formation of cation-binding pockets. *Nucl. Acids Res.* **31**, 6942–6952.
35. Auffinger, P., Bielecki, L. & Westhof, E. (2003). The Mg^{2+} binding sites of the 5S rRNA loop E motif as investigated by molecular dynamics simulations. *Chem. Biol.* **10**, 551–561.
36. Sanbonmatsu, K. Y. & Joseph, S. (2003). Understanding discrimination by the ribosome: stability testing and groove measurement of codon-anticodon pairs. *J. Mol. Biol.* **328**, 33–47.
37. Beaurain, F., Di Primo, C., Toulme, J. J. & Laguerre, M. (2003). Molecular dynamics reveals the stabilizing role of loop closing residues in kissing interactions: comparison between TAR-TAR* and TAR-aptamer. *Nucl. Acids Res.* **31**, 4275–4284.
38. Orozco, M., Perez, A., Noy, A. & Luque, F. J. (2003). Theoretical methods for the simulation of nucleic acids. *Chem. Soc. Rev.* **32**, 350–364.
39. Auffinger, P., Bielecki, L. & Westhof, E. (2004). Symmetric K^+ and Mg^{2+} ion-binding sites in the 5S rRNA loop E inferred from molecular dynamics simulations. *J. Mol. Biol.* **335**, 555–571.
40. Razga, F., Koca, J., Sponer, J. & Leontis, N. B. (2005). Hinge-like motions in RNA kink-turns: the role of the second A-minor motif and nominally unpaired bases. *Biophys. J.* **88**, 3466–3485.
41. Hermann, T., Auffinger, P., Scott, W. G. & Westhof, E. (1997). Evidence for a hydroxide ion bridging two magnesium ions at the active site of the hammerhead ribozyme. *Nucl. Acids Res.* **25**, 3421–3427.
42. Hermann, T., Auffinger, P. & Westhof, E. (1998). Molecular dynamics investigations of hammerhead ribozyme RNA. *Eur. Biophys. J.* **27**, 153–165.
43. Torres, R. A. & Bruice, T. C. (1998). Molecular dynamics study displays near in-line attack conformations in the hammerhead ribozyme self-cleavage reaction. *Proc. Natl Acad. Sci. USA*, **95**, 11077–11082.
44. Torres, R. A. & Bruice, T. C. (2000). The mechanism of phosphodiester hydrolysis: near in-line attack conformations in the hammerhead ribozyme. *J. Am. Chem. Soc.* **122**, 781–791.
45. Boero, M., Terakura, K. & Tateno, M. (2002). Catalytic role of metal ion in the selection of competing reaction paths: A first principles molecular dynamics study of the enzymatic reaction in ribozyme. *J. Am. Chem. Soc.* **124**, 8949–8957.
46. Varnai, P. & Zakrzewska, K. (2004). DNA and its counterions: a molecular dynamics study. *Nucl. Acids Res.* **32**, 4269–4280.
47. Rueda, M., Cubero, E., Laughton, C. A. & Orozco, M. (2004). Exploring the counterion atmosphere around DNA: what can be learned from molecular dynamics simulations? *Biophys. J.* **87**, 800–811.
48. Nissen, P., Ippolito, J. A., Ban, N., Moore, P. B. & Steitz, T. A. (2001). RNA tertiary interactions in the large ribosomal subunit: the A-minor motif. *Proc. Natl Acad. Sci. USA*, **98**, 4899–4903.
49. Leontis, N. B., Stombaugh, J. & Westhof, E. (2002). The non-Watson–Crick base-pairs and their associated isostericity matrices. *Nucl. Acids Res.* **30**, 3497–3531.
50. Bevilacqua, P. C., Brown, T. S., Nakano, S. & Yajima, R. (2004). Catalytic roles for proton transfer and protonation in ribozymes. *Biopolymers*, **73**, 90–109.
51. Nixon, P. L., Rangan, A., Kim, Y. G., Rich, A., Hoffman, D. W., Hennig, M. & Giedroc, D. P. (2002). Solution structure of a luteoviral P1-P2 frameshifting mRNA pseudoknot. *J. Mol. Biol.* **322**, 621–633.
52. Nissen, P., Hansen, J., Ban, N., Moore, P. B. & Steitz, T. A. (2000). The structural basis of ribosome activity in peptide bond synthesis. *Science*, **289**, 920–930.
53. Muth, G. W., Ortoleva-Donnelly, L. & Strobel, S. A. (2000). A single adenosine with a neutral pKa in the ribosomal peptidyl transferase center. *Science*, **289**, 947–950.
54. Rupert, P. B. & Ferre-D'Amare, A. R. (2001). Crystal structure of a hairpin ribozyme–inhibitor complex with implications for catalysis. *Nature*, **410**, 780–786.
55. Pinard, R., Hampel, K. J., Heckman, J. E., Lambert, D., Chan, P. A., Major, F. & Burke, J. M. (2001). Functional involvement of G8 in the hairpin ribozyme cleavage mechanism. *EMBO J.* **20**, 6434–6442.
56. Muth, G. W., Chen, L., Kosek, A. B. & Strobel, S. A. (2001). pH-dependent conformational flexibility within the ribosomal peptidyl transferase center. *RNA*, **7**, 1403–1415.
57. Polacek, N., Gaynor, M., Yassin, A. & Mankin, A. S. (2001). Ribosomal peptidyl transferase can withstand mutations at the putative catalytic nucleotide. *Nature*, **411**, 498–501.
58. Katunin, V. I., Muth, G. W., Strobel, S. A., Wintermeyer, W. & Rodnina, M. V. (2002). Important contribution to catalysis of peptide bond formation by a single ionizing group within the ribosome. *Mol. Cell*, **10**, 339–346.
59. Youngman, E. M., Brunelle, J. L., Kochaniak, A. B. & Green, R. (2004). The active site of the ribosome is composed of two layers of conserved nucleotides with distinct roles in peptide bond formation and peptide release. *Cell*, **117**, 589–599.
60. Weinger, J. S., Parnell, K. M., Dorner, S., Green, R. & Strobel, S. A. (2004). Substrate-assisted catalysis of peptide bond formation by the ribosome. *Nature Struct. Mol. Biol.* **11**, 1101–1106.
61. Sievers, A., Beringer, M., Rodnina, M. V. & Wolfenden, R. (2004). The ribosome as an entropy trap. *Proc. Natl Acad. Sci. USA*, **101**, 7897–7901.
62. Rupert, P. B., Massey, A. P., Sigurdsson, S. T. & Ferre-D'Amare, A. R. (2002). Transition state stabilization by a catalytic RNA. *Science*, **298**, 1421–1424.
63. Kuzmin, Y. I., Da Costa, C. P. & Fedor, M. J. (2004). Role of an active site guanine in hairpin ribozyme catalysis probed by exogenous nucleobase rescue. *J. Mol. Biol.* **340**, 233–251.
64. Hobza, P., Kabelac, M., Sponer, J., Mejzlik, P. & Vondrasek, J. (1997). Performance of empirical potentials (AMBER, CFF95, CVFF, CHARMM, OPLS, POLTEV), semi-empirical quantum chemical methods (AM1, MNDO/M, PM3), and *ab initio* Hartree–Fock method for interaction of DNA bases: comparison with non-empirical beyond Hartree–Fock results. *J. Comput. Chem.* **18**, 1136–1150.
65. Reblova, K., Spackova, N., Koca, J., Leontis, N. B. & Sponer, J. (2004). Long-residency hydration, cation binding, and dynamics of loop E/helix IV rRNA-L25 protein complex. *Biophys. J.* **87**, 3397–3412.
66. Schneider, B., Moravek, Z. & Berman, H. M. (2004). RNA conformational classes. *Nucl. Acids Res.* **32**, 1666–1677.
67. Case, D. A., Pearlman, D. A., Caldwell, J. W., Cheathan, T. E., III, Wang, J., Ross, W. S. *et al*. (2002). *AMBER 7*, University of California San Francisco, San Francisco.
68. Cornell, W. D., Cieplak, P., Bayly, C. I., Gould, I. R., Merz, K. M., Ferguson, D. M. *et al*. (1995). A 2nd

generation force-field for the simulation of proteins, nucleic-acids, and organic-molecules. *J. Am. Chem. Soc.* **117**, 5179–5197.
69. Wang, J. M., Cieplak, P. & Kollman, P. A. (2000). How well does a restrained electrostatic potential (RESP) model perform in calculating conformational energies of organic and biological molecules? *J. Comput. Chem.* **21**, 1049–1074.
70. Cheatham, T. E., Cieplak, P., Kollman, P. A. *et al.* (1999). A modified version of the Cornell *et al.* force field with improved sugar pucker phases and helical repeat. *J. Biomol. Struct. Dynam.* **16**, 845–862.
71. Jorgensen, W. L., Chandrasekhar, J., Madura, J. D., Impey, R. W. & Klein, M. L. (1983). Comparison of simple potential functions for simulating liquid water. *J. Chem. Phys.* **79**, 926–935.
72. Aqvist, J. (1990). Ion water interaction potentials derived from free-energy perturbation simulations. *J. Phys. Chem.* **94**, 8021–8024.
73. Spackova, N., Berger, I. & Sponer, J. (2001). Structural dynamics and cation interactions of DNA quadruplex molecules containing mixed guanine/cytosine quartets revealed by large-scale MD simulations. *J. Am. Chem. Soc.* **123**, 3295–3307.
74. Essmann, U., Perera, L., Berkowitz, M. L., Darden, T., Lee, H. & Pedersen, L. G. (1995). A smooth particle mesh Ewald method. *J. Chem. Phys.* **103**, 8577–8593.
75. Berendsen, H. J. C., Postma, J. P. M., Vangunsteren, W. F., Dinola, A. & Haak, J. R. (1984). Molecular-dynamics with coupling to an external bath. *J. Chem. Phys.* **81**, 3684–3690.
76. Ryckaert, J. P., Ciccotti, G. & Berendsen, H. J. C. (1977). Numerical integration of the Cartesian equations of motion of a system with constraints: molecular dynamics of *n*-alkanes. *J. Comput. Chem.* **23**, 327–341.
77. Humphrey, W., Dalke, A. & Schulten, K. (1996). VMD: visual molecular dynamics. *J. Mol. Graph.* **33**, 33.
78. Gelpi, J. L., Kalko, S. G., Barril, X., Cirera, J., de la Cruz, X., Luque, F. J. & Orozco, M. (2001). Classical molecular interaction potentials: improved setup procedure in molecular dynamics simulations of proteins. *Proteins: Struct. Funct. Genet.* **45**, 428–437.

Edited by J. Doudna

(Received 17 January 2005; received in revised form 31 May 2005; accepted 7 June 2005)
Available online 24 June 2005